



**NAVAL
POSTGRADUATE
SCHOOL**

MONTEREY, CALIFORNIA

**SHORT RANGE WIRELESS POWER TRANSFER (WPT) FOR
UAV/UAS BATTERY CHARGING – PHASE I**

by

David Jenn

December 2014

Approved for public release; distribution is unlimited

Prepared for:

Consortium for Robotics and Unmanned Systems Education and Research (CRUSER)

THIS PAGE INTENTIONALLY LEFT BLANK

REPORT DOCUMENTATION PAGE				<i>Form Approved</i> OMB No. 0704-0188	
Public reporting burden for this collection of information is estimated to average 1 hour per response, including the time for reviewing instructions, searching existing data sources, gathering and maintaining the data needed, and completing and reviewing this collection of information. Send comments regarding this burden estimate or any other aspect of this collection of information, including suggestions for reducing this burden to Department of Defense, Washington Headquarters Services, Directorate for Information Operations and Reports (0704-0188), 1215 Jefferson Davis Highway, Suite 1204, Arlington, VA 22202-4302. Respondents should be aware that notwithstanding any other provision of law, no person shall be subject to any penalty for failing to comply with a collection of information if it does not display a currently valid OMB control number. PLEASE DO NOT RETURN YOUR FORM TO THE ABOVE ADDRESS.					
1. REPORT DATE (DD-MM-YYYY) 01-12-2014		2. REPORT TYPE Technical Report		3. DATES COVERED (From-To) 1/1/2014 to 12/31/2014	
4. TITLE AND SUBTITLE Short Range Wireless Power Transfer (WPT) for UAV/UAS Battery Charging – Phase I				5a. CONTRACT NUMBER	
				5b. GRANT NUMBER	
				5c. PROGRAM ELEMENT NUMBER	
6. AUTHOR(S) David Jenn				5d. PROJECT NUMBER	
				5e. TASK NUMBER	
				5f. WORK UNIT NUMBER	
7. PERFORMING ORGANIZATION NAME(S) AND ADDRESS(ES) AND ADDRESS(ES) Department of Electrical and Computer Engineering				8. PERFORMING ORGANIZATION REPORT NUMBER NPS-EC-14-004	
9. SPONSORING / MONITORING AGENCY NAME(S) AND ADDRESS(ES) CRUSER				10. SPONSOR/MONITOR'S ACRONYM(S)	
				11. SPONSOR/MONITOR'S REPORT NUMBER(S)	
12. DISTRIBUTION / AVAILABILITY STATEMENT Approved for public release; distribution is unlimited					
13. SUPPLEMENTARY NOTES					
14. ABSTRACT The inductive and radiative approaches to wireless power transmission (WPT) were simulated using commercial software. For the inductive approach, working at 100 kHz, efficiencies over 90% were obtained at short ranges (less than 30 mm) utilizing ferrite plates. For the radiative approach, the transmission loss between antennas was less than 1 dB at ranges less than 3 m when near field focusing was employed. The results for the two approaches are important because they demonstrate that efficient transmission of energy for battery charging can take place between a WPT ground station and client.					
15. SUBJECT TERMS Wireless power transmission, phased array, inductive WPT, radiative WPT					
16. SECURITY CLASSIFICATION OF:			17. LIMITATION OF ABSTRACT UU	18. NUMBER OF PAGES 35	19a. NAME OF RESPONSIBLE PERSON David Jenn
a. REPORT Unclassified	b. ABSTRACT Unclassified	c. THIS PAGE Unclassified			

Standard Form 298 (Rev. 8-98)
Prescribed by ANSI Std. Z39.18

THIS PAGE INTENTIONALLY LEFT BLANK

**NAVAL POSTGRADUATE SCHOOL
Monterey, California 93943-5000**

Ronald A. Route
President

Douglas A. Hensler
Provost

The report entitled “Short Range Wireless Power Transfer (WPT) for UAV/UAS Battery Charging – Phase I” was prepared for and funded by Consortium for Robotics and Unmanned Systems Education and Research (CRUSER).

Further distribution of all or part of this report is authorized.

This report was prepared by:

David C. Jenn
Professor

Reviewed by:

R. Clark Robertson, Chairman
Department of Electrical and
Computer Engineering

Released by:

Jeffrey D. Paduan
Dean of Research

THIS PAGE INTENTIONALLY LEFT BLANK

ABSTRACT

The inductive and radiative approaches to wireless power transmission (WPT) were simulated using commercial software. For the inductive approach, working at 100 kHz, efficiencies over 90% were obtained at short ranges (less than 30 mm) utilizing ferrite plates. For the radiative approach, the transmission loss between antennas was less than 1 dB at ranges less than 3 m when near field focusing was employed. The results for the two approaches are important because they demonstrate that efficient transmission of energy for battery charging can take place between a WPT ground station and client.

THIS PAGE INTENTIONALLY LEFT BLANK

I. INTRODUCTION

A. BACKGROUND

There are numerous advantages of wireless power transfer (WPT) for many remote energy source and battery charging applications. The approach was first proposed for vehicle propulsion in mid 1960s and shortly after demonstrated by researchers at Raytheon [1]. It gained renewed interest in the early 1990s for micro-UAV propulsion. More recently, WPT has been used for charging wireless devices, and commercial WPT charging products have appeared on the market (for example, *Witricity* and *Energous*¹).

The basic block diagram of a WPT system is shown in Figure 1. Prime power is provided by the base station (master), converted to radio frequency (RF) and then input to a coil or antenna. On the client side the received power is conditioned (filtered and transformed in voltage and current) and subsequently delivered to the battery or power plant.

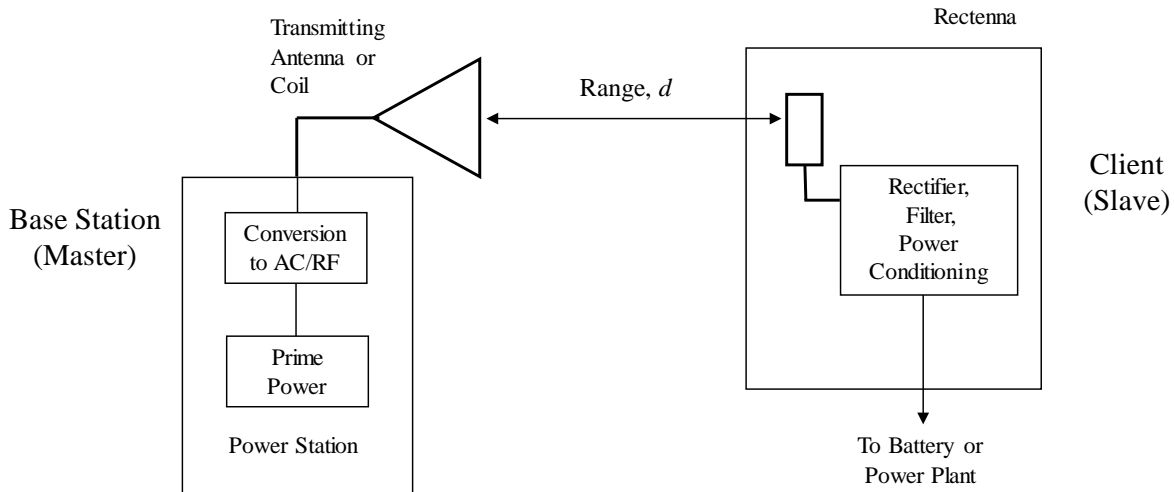


Figure 1. Block diagram of a WPT system for battery charging.

There are two broad approaches to the problem based on the operating range (distance) of interest. They are the inductive and far-field (radiative) regimes.

B. INDUCTIVE APPROACH

For short ranges (less than a couple of cm) inductive WPT systems are viable. Inductive systems use two coils (as shown in Figure 2) with one located in the charging station and the second in the device. Energy is transferred by the magnetic fields linking the coils. Essentially it is a transformer without a core material. At the receiving coil, circuits are required to rectify and condition the output voltage for charging the battery.

¹ See <http://www.witricity.com/> and <http://energous.com/>

Inductive systems generally operate at low frequencies (< 10 MHz and usually in the hundreds of kHz range). Efficiencies greater than 75% are routinely achieved, with some systems achieving efficiencies greater than 95%, however, they operate at very short ranges (several mm). The short range can limit the application of WPT and furthermore alignment and spacing of the coils is critical.

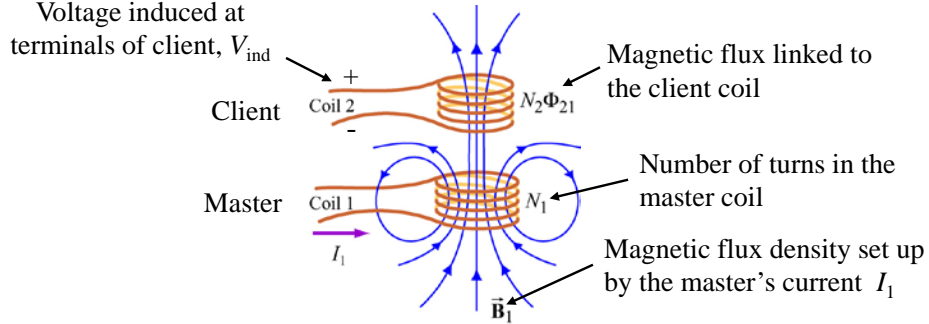


Figure 2: Inductive power transfer (after [2]).

The transfer of power is governed by Faraday's Law [2], which gives the induced voltage in the client coil as

$$V_{\text{ind}} = -\frac{N_2 d\Phi_{21}}{dt} \quad (1)$$

where Φ_{21} is the magnetic flux set up by the current in the master coil that is linked to the client coil. The linked magnetic flux is a complex function of the coil geometries, size, frequency of operation f , and distance. Generally it is not possible to compute Φ_{21} in closed form except for some very simple cases. However, electromagnetic simulation software is capable of numerically solving for the currents and voltages in the WPT circuit.

C. RADIATIVE APPROACH

Radiative WPT systems use two antennas rather than coils, and the energy is transferred by a propagating wave, as depicted in Figure 3. The received power at antenna separation d is given by the Friis equation [2]:

$$P_r = \frac{P_t G_t G_r \lambda^2 L}{(4\pi d)^2} |F|^2 \quad (2)$$

where P_t is the transmitted power, G_t the charging station antenna gain, G_r the receiving (client) antenna gain, and $\lambda=c/f$ is the wavelength (c is the speed of light, f is the frequency in Hz). F is a factor that accounts for wave propagation effects in the medium, such as multipath and attenuation. L is a system loss factor that includes device losses, rectifier efficiency, etc. The receive side the antenna has an integrated rectifier, and is called a rectenna.

Radiative systems operate at higher frequencies than inductive systems (> 1 GHz), and suffer a $1/d^2$ propagation loss. Normally d must be great enough so that the antennas are in each other's far field region. Higher gain antennas can be used to increase the received power, but high gain antennas have a farther near-field boundary, and they become physically larger. The

use of antennas has advantages though. Solid state array antennas allow full control of the antenna excitation, which permits scanning and focusing of the beam. This capability relaxes the alignment requirements between the two antennas, and can be employed to improve the system performance when the antenna far-field criteria are not met.

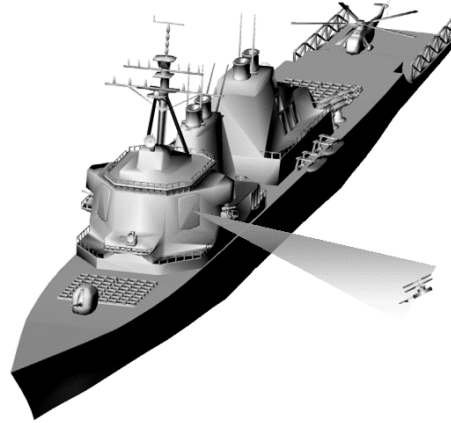


Figure 3: Example of a radiative WPT system (i.e., “microwave beaming” from a transmitting radar).

A disadvantage of radiative systems is that they are more susceptible to losses in the medium (i.e. attenuation). In clear air there is no significant attenuation for frequencies less than 15 GHz. To keep the losses acceptable, a clear line-of-sight (LOS) in air is desirable. Therefore, this approach cannot be used for vehicles submerged in water or buried in wet ground. However, it can be used for ground vehicles, air vehicles on the ground, or even warfighter packed equipment. It does not require the precise alignment of the charging station and client, and can be designed to operate at distances of several meters or more.

D. SAFETY AND INTERFERENCE

Other issues that must be considered when using electromagnetic energy are safety and interference. Radiative systems are more directive than inductive systems (significant power in the main beam; negligible power outside of the main beam). The low frequencies used by inductive systems penetrate materials more readily, including the human body. However, because of the short ranges and relatively low power involved, safety should not be an issue. Both types of systems can cause interference in neighboring electronic systems. Again, because of the short range of the systems, the interference introduced by a practical system should be limited to same platform (self) interference.

THIS PAGE INTENTIONALLY LEFT BLANK

II. INDUCTIVE WPT STUDY

A. SYSTEM DESIGN

We have investigated an inductive WPT system for charging underwater vehicles [3]. The concept has been studied previously by SSC Pacific in San Diego [4]. It is a short range (< 4 cm) system that operates at 100 kHz. The low frequency is dictated by the requirement that the system operates efficiently through seawater.

There are four types of compensation network combinations that can be used: 1) series-series, 2) series-parallel, 3) parallel-series, and 4) parallel-parallel. Two types of compensation networks are shown in Figure 4. We have selected the series-series approach because of its simplicity, and it is the topology used by SSC Pacific.

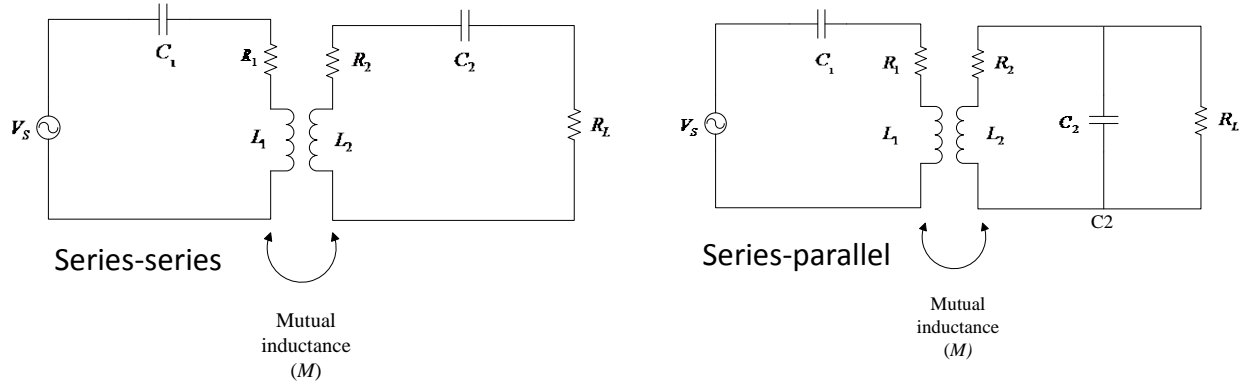


Figure 4: Equivalent circuit of the inductive WPT system with two types of compensation networks.

The efficiency is the power delivered to the load relative to the power transmitted [3]:

$$\eta = \frac{P_L}{P_t} = \frac{R_L(\omega_0 M)^2}{R_1(R_2 + R_L)^2 + (\omega_0 M)^2(R_2 + R_L)} \quad (3)$$

where

- V_s , Voltage supply,
- R_1 , Internal resistance of the transmitting coil,
- R_2 , Internal resistance of the receiving coil,
- L_1 , Inductance of transmitting coil,
- L_2 , Inductance of the receiving coil,
- C_1 , Compensating capacitance for the transmitting coil,
- C_2 , Compensating capacitance for the receiving coil,
- I_1 , Transmitting coil current,
- I_2 , Receiving coil current, and
- M , Mutual inductance between the transmitting and receiving coils.

The magnetic coupling coefficient expresses how well the transmitting and receiving coils are magnetically coupled together. The higher the value of k the better the magnetic coupling is between the two coils. The magnetic coupling coefficient is defined as

$$k \equiv \frac{M}{\sqrt{L_1 L_2}}. \quad (4)$$

We can show that there is an ideal matched load resistance for a given gap (coil spacing). The resulting $R_{L,matched}$ can be expressed as

$$R_{L,matched} = \sqrt{R_2^2 + (\omega M)^2 \frac{R_2}{R_1}}. \quad (5)$$

From Eq. (5) it is apparent that the matched load changes with distance (through M). Mutual coupling M (and hence k which depends on M) are not easily computed, and must be determined by simulation or measurement.

Several commercial software packages can be used to simulate the WPT circuit and coils. CST *Microwave Studio* was selected. The frequency domain solver was used to find the voltage and current at the load for a known applied voltage at the input. The numerical solver provides a rigorous solution of Maxwell's equations for the specified boundary conditions. However some numerical errors are present because of the meshing and other approximations in evaluating equations. In most cases these errors can be made as small as desired at the cost of increased simulation time and memory requirements.

The MWS model is shown in Figure 5(a). The coils are backed by plates and have cores. The plates and cores are shown in blue, which is set as free space initially to model the coils in air. The efficiency is given by [3]

$$\eta = \frac{P_L}{P_{in}} = \frac{|V_L|^2 / R_L}{|V_{in}|^2 |I_{in}|^2 \cos \theta} \quad (6)$$

where V_L = voltage across the load

V_{in} = voltage across the input

I_{in} = current at the input

$\cos \theta$ = power factor (cosine of phase angle of voltage minus phase angle of current).

B. SIMULATIONS AND MEASUREMENTS

The computed efficiency is shown in Figure 5(b) for the coils in air with a spacing of 16 mm (face to face). The computed optimum load value is 29 Ω . The optimum load was computed from the dimensions of the coils used in the lab measurements, which are only approximated in the MWS model. (It is not possible to model wires in MWS as thin as those used in the actual coils.) From the simulation data the optimum appears to be about 45 Ω .

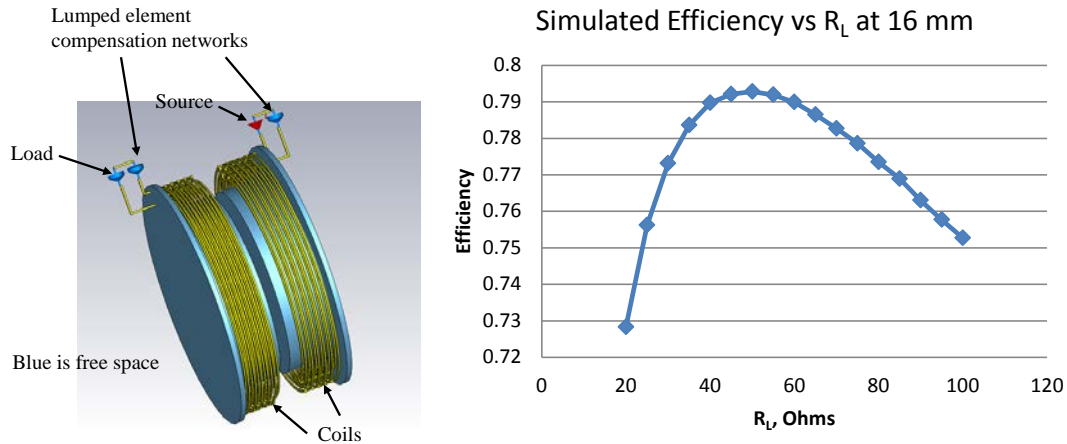


Figure 5: (a) CST MWS model of the WPT coils and circuit, and (b) simulated efficiency versus load resistance.

Measurements were performed in the Microwave Laboratory by Cena [3] and the results are reported in his thesis. The measurement setup is shown in Figure 6(a) and the results summarized in Figure 7. At 16 mm spacing the simulated and measured data are in close agreement, but both are slightly below the calculated value. See [3] for details on the calculated value.

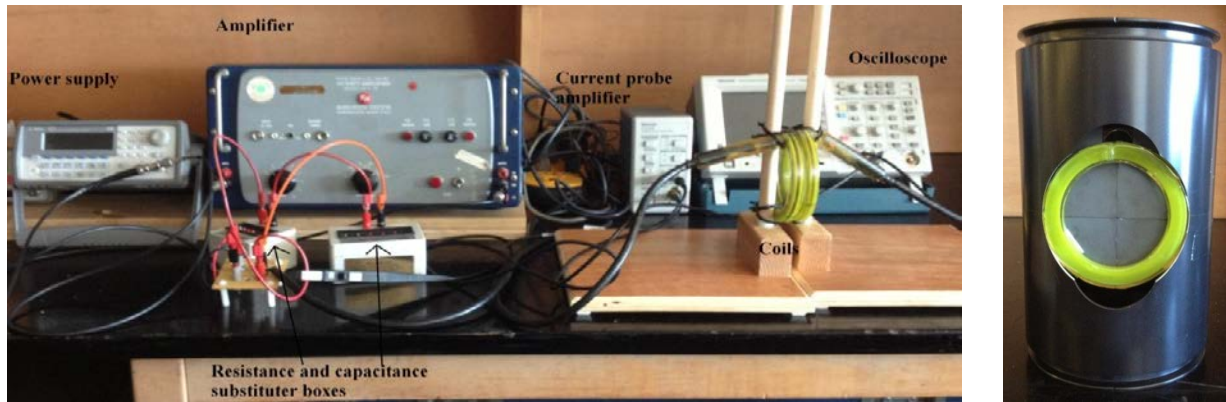


Figure 6: (a) Measurement setup used to obtain efficiency, and (b) coil installed in a UAV hull (from [3]).

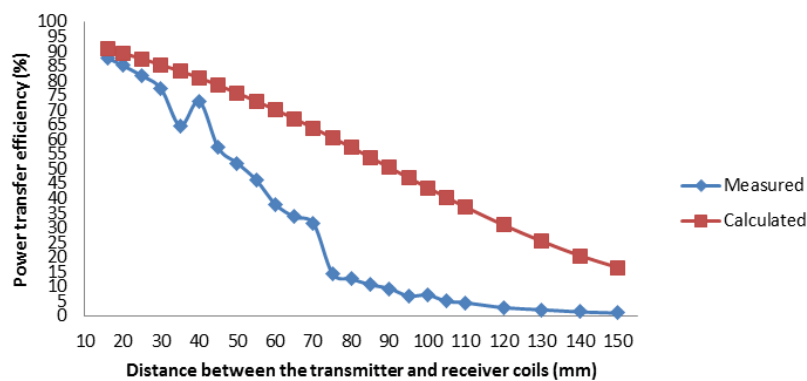


Figure 7: Summary of efficiency results based on measured data (from [3]).

A way to confine the magnetic flux and increase coupling is to add a ferrite surface behind the receiving coil. The placement of the ferrite board behind the receiving coil was suggested by SSC Pacific. The effect of a ferrite plate is illustrated in the plots shown in Figure 8. The magnet, which is equivalent to a current loop, represents the transmitting coil. The long rectangle on the right is the location of the ferrite tile and is assigned $\mu_r = 1$. A relative magnetic permeability of 1 represents a WPT system without ferrite tiles. In Figure 8(b), the long rectangle on the right is assigned $\mu_r = 20$ which represents a system with ferrite tiles. The concentration of the magnetic field in the red area (location of the receiving coil) is apparent when comparing the two figures. The plots in were created using Vizimag 3.18.

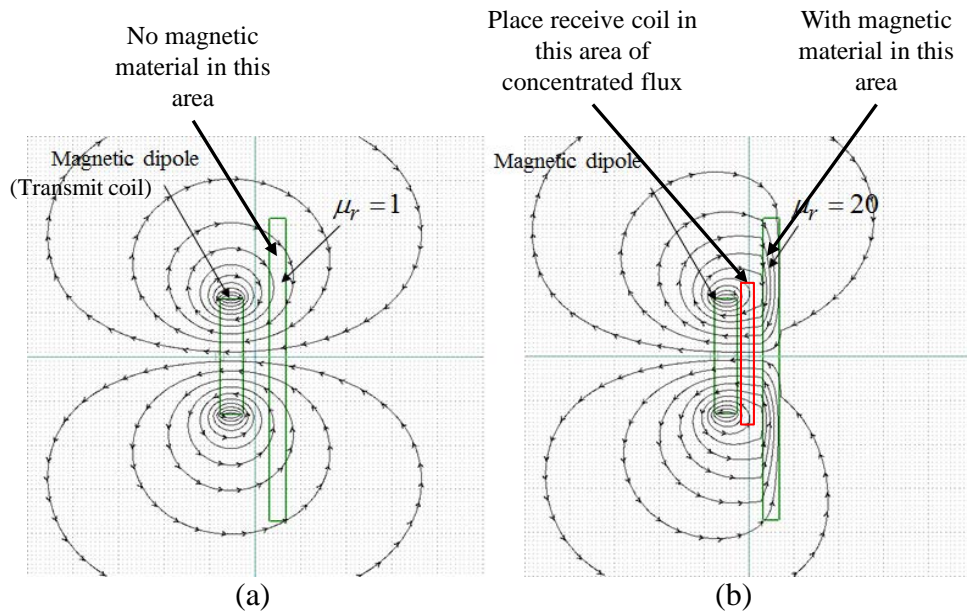


Figure 8: Application of ferrite plates to concentrate the magnetic flux (after [3]).

MWS simulations were performed with ferrite plates and cores. A sample of the results is shown in Figure 9 as a function of load resistance. The simulations can be used to find the optimum load resistance from the peaks of the efficiency curves. Note that the efficiency is improved using both the ferrite plates and cores. It was also found that increasing the permeability of the tiles improved the efficiency and reduced the efficiency's dependency on the load value. However, a small efficiency improvement (e.g., less than 10 %) may not be worth the cost in terms of weight and complexity.

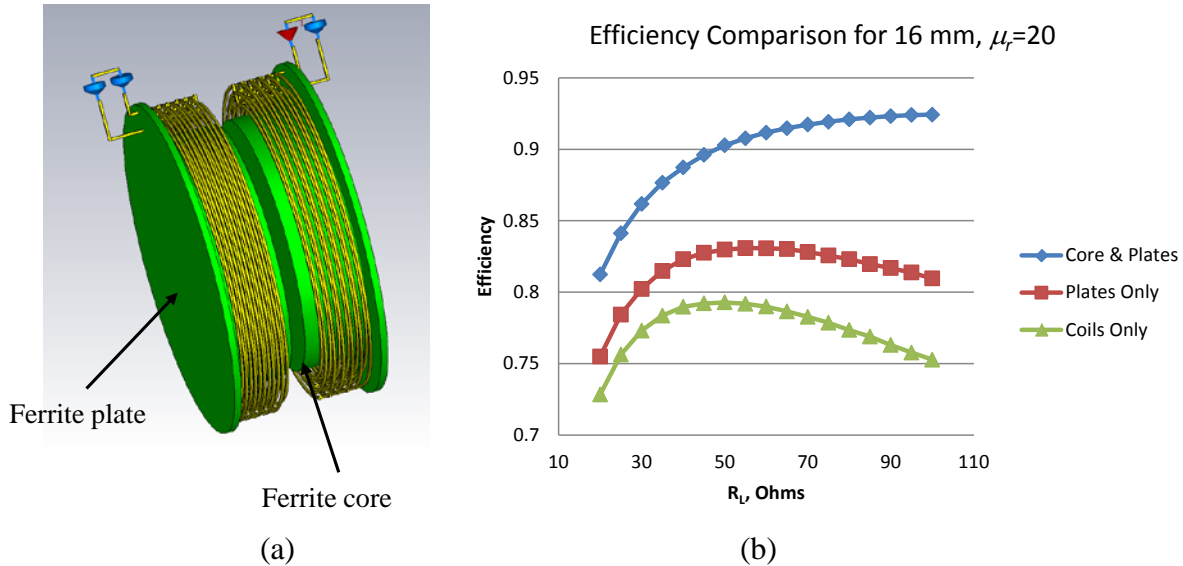


Figure 9: Simulation results for coils with ferrite cores and plates.

Measurements were taken by Cena with ferrite plates behind the receiving antenna. The plate arrangement and a summary of the results are shown in Figure 10. The number of available tiles was limited, which forced the irregular arrangement shown in Figure 10(b). The measured data also showed an increase in efficiency using the tiles compared to air.

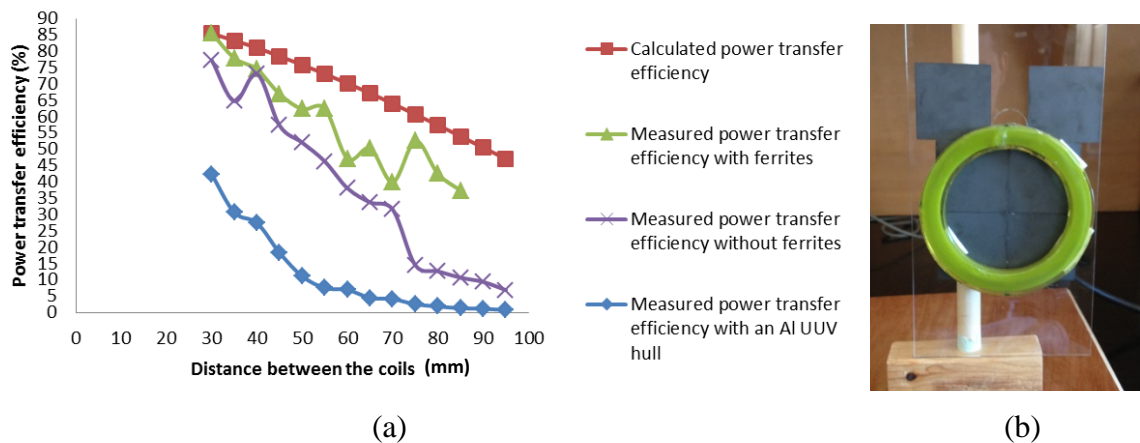


Figure 10: Measured results with ferrite cores (from [3]).

C. SUMMARY OF INDUCTIVE WPT

The measurements and simulations of inductive WPT have shown that high efficiencies can be obtained at close coil spacing. A frequency of 100 kHz was used to allow the system to operate in seawater without suffering decreased efficiency due to the water resistance. The next phase of research should concentrate on designing a practical interface between the coils, and optimization of the rectifying and charging circuit.

THIS PAGE INTENTIONALLY LEFT BLANK

III. RADIATIVE WPT STUDY

A. SYSTEM DESIGN

In a radiative system, the master station transmits a propagating electromagnetic wave to the client. Generally the master station has a high gain antenna that must be continuously pointed in the direction of the client. This type of WPT has been proposed for numerous applications such as space based power (Figure 11), battery charging, spacecraft recharging and station keeping, and direct propulsion of UAVs and hovering airships. The client antenna is usually of low gain and small physical size because it operates on a mobile platform (e.g., UAV).



Figure 11: Space solar power (SSP) concept whereby energy collected by solar panels is transmitted to Earth at microwave frequencies (from [5]).

Equation (2) governs the received power versus the system parameters. The antenna gains are given by [2]

$$G = 4\pi A_e / \lambda^2 \quad (7)$$

where $A_e = Ae_a$, effective area

A = aperture area (m^2)

e_a = antenna efficiency ($0 \leq e_a \leq 1$)

$\theta_B \approx \lambda / L$, half-power beamwidth (HBPW) in radians in the principal plane where the dimension is L .

B. NEAR FIELD FORMULATION

1. Transmitting Array

At close distances the antennas may be in each other's near field. In the near-field, the full gain of the antennas will not be achieved if uniform amplitude and phase weighting is employed. If the master station antenna is an array with full amplitude and phase control at the element level, then near-field focusing can be used. Figure 12 shows the near-field operation. For a general case, let the array focal point be at $\vec{r}_f(x_f, y_f, z_f)$ and the observation (field point) at

$\vec{R}(x, y, z)$. (Note that here R is not a resistance, but the standard spherical polar radial variable.) The array is located in the x - z plane and has a rectangular grid with N_x by N_z elements ($1 \leq m \leq N_x$ and $1 \leq n \leq N_z$) spaced d_x by d_z . The normal vector to the array is \hat{y} .

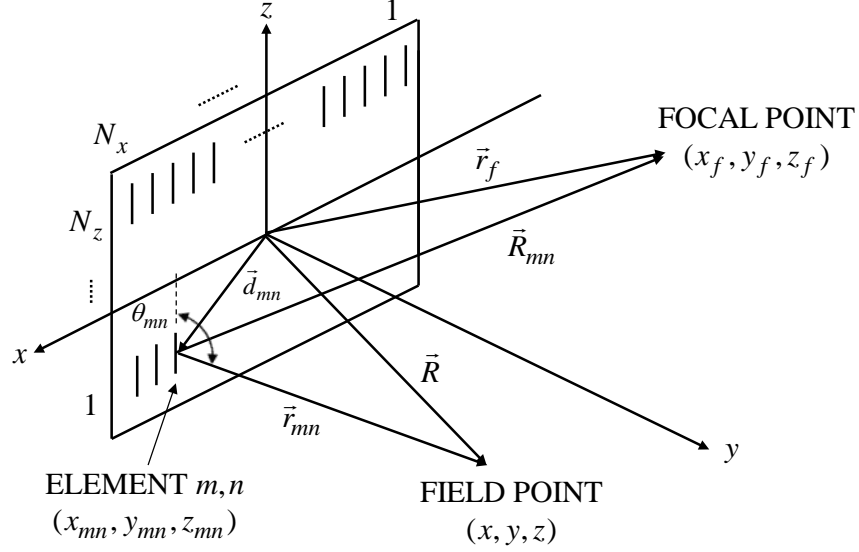


Figure 12. Planar array antenna near field model.

Other parameters of interest are:

- The position vector to element m,n : $\vec{d}_{mn} = x_{mn}\hat{x} + z_{mn}\hat{z}$ where $x_{mn} = \frac{2m - (N_x + 1)}{2}d_x$, $z_{mn} = \frac{2n - (N_z + 1)}{2}d_z$, and $y_{mn} = 0$.
- Position vector to the focal point: $\vec{r}_f = x_f\hat{x} + y_f\hat{y} + z_f\hat{z}$.
- Position vector to the observation point: $\vec{R} = x\hat{x} + y\hat{y} + z\hat{z}$.
- Vector from element m,n to the focal point:

$$\vec{R}_{mn} = (x_f - x_{mn})\hat{x} + (y_f - y_{mn})\hat{y} + (z_f - z_{mn})\hat{z}. \quad (8)$$

- Vector from element m,n to the field point:

$$\vec{r}_{mn} = (x - x_{mn})\hat{x} + (y - y_{mn})\hat{y} + (z - z_{mn})\hat{z} \quad (9)$$

so that $\hat{r}_{mn} = \frac{\vec{r}_{mn}}{|\vec{r}_{mn}|}$.

Let the elements be z -directed and linearly polarized. A general form for the element factor is

$$\vec{F}_{mn}(\theta_{mn}, \phi_{mn}) = \hat{z} C_o \cdot \Psi(r_{mn}) \cdot f_{mn}(\theta_{mn}, \phi_{mn}) \quad (10)$$

where:

- $f_{mn}(\theta_{mn}, \phi_{mn})$ is the normalized element pattern as a function of angles θ_{mn}, ϕ_{mn} .

- $\Psi(r_{mn}) = \frac{e^{-j\beta r_{mn}}}{r_{mn}}$ is the free space Green's function with $\beta = 2\pi / \lambda$.
- C_o a complex constant that depends on the element type (e.g., dipole, patch, etc.).
- θ_{mn} is the angle between the element m,n axis (along z) and the field point position vector:

$$\cos \theta_{mn} = \hat{z} \cdot \hat{r}_{mn}, \quad \sin \theta_{mn} = \sqrt{1 - \cos^2 \theta_{mn}} \quad (11)$$

ϕ_{mn} is the element azimuth angle:

$$\tan \phi_{mn} = \frac{y_f - y_{mn}}{x_f - x_{mn}}. \quad (12)$$

To this point we have allowed for the patterns of each element to be different. Typically all elements are the same so that $\vec{F}_{mn}(\theta_{mn}, \phi_{mn}) \equiv \vec{F}(\theta_{mn}, \phi_{mn})$ or $f_{mn}(\theta_{mn}, \phi_{mn}) \equiv f(\theta_{mn}, \phi_{mn})$. If the elements are unit current amplitude z -directed half-wave dipoles at height h above a ground plane that is a perfect electrical conductor (PEC), then the ground plane element factor is

$$\vec{F}(\theta_{mn}, \phi_{mn}) = j120 \hat{z} \underbrace{\frac{e^{-j\beta r_{mn}}}{r_{mn}}}_{\Psi(r_{mn})} \underbrace{\frac{\cos\left(\frac{\pi}{2} \cos \theta_{mn}\right)}{\sin \theta_{mn}} \sin(\beta h \sin \theta_{mn} \sin \phi_{mn})}_{f(\theta_{mn}, \phi_{mn})}. \quad (13)$$

In (13) the far-field condition has been assumed for the ground plane factor. This is an idealized result for an isolated element above an infinite ground plane. The ground plane factor for a dipole over a finite ground plane, or in an array environment, or in the near field will differ from $\sin(\beta h \sin \theta_{mn} \sin \phi_{mn})$ due to mutual coupling and diffraction. These effects can be accounted for by modifying the ground plane factor as described in the Appendix.

The total array field at the observation point is given by the weighted sum

$$\begin{aligned} \vec{E}(R, \theta, \phi) &= \sum_{m=1}^{N_x} \sum_{n=1}^{N_z} A_{mn} e^{j\Phi_{mn}} e^{j\psi_{mn}} \vec{F}(\theta_{mn}, \phi_{mn}) \\ &= j120 \hat{z} \sum_{m=1}^{N_x} \sum_{n=1}^{N_z} \left\{ \frac{e^{-j\beta r_{mn}}}{r_{mn}} f(\theta_{mn}, \phi_{mn}) A_{mn} e^{j\Phi_{mn}} e^{j\psi_{mn}} \right\} \end{aligned} \quad (14)$$

where

- A_{mn} is the element's current amplitude coefficient.
- Φ_{mn} is the phase required to focus the beam at r_f :

$$\Phi_{mn} = \beta(r_f - r_{mn}). \quad (15)$$

- ψ_{mn} is a miscellaneous calibration and correction phase.

In Figures 13 and 14 we plot the electric field intensity for an array of half-wave dipoles above a ground plane with the parameters in Table 1.

Table 1. Parameters for the plots in Figures 13 and 14 (extracted from Matlab script)

```
f=10e9; % frequency
wave=3e8/f;
% Observation parameters
Xmax=2; % -Xmax to Xmax
Ymax=6; % DZ to Zmax to avoid singularity
zp=0; % observation plane height
% Array Parameters
Nx=30; Nz=20;
dx=0.5*wave; dz=0.5*wave;
hgp=0.25*wave;
```

The subtle variations in the field distribution are more easily seen if the free space attenuation of the field is removed. Thus at an observation point a distance R from the origin

$$E_{\text{norm}} = \frac{R|E(R, \theta, \phi)|}{|E(R, \theta, \phi)|_{\text{max}}} \quad \text{or in dB: } 20\log_{10}|E_{\text{norm}}|. \quad (16)$$

In Figure 13 is shown a plot of the normalized electric field intensity in V/m and dBV/m when the transmit array is focused at 2 m. In Figure 14 the result shown is for the focal point at 2000 m, which is in the array's far field (i.e., a linear phase is used to scan the beam). The black stem is located at the focal point. It is clear that the field reaches a maximum at the focal point in Figure 13, whereas that is not the case in Figure 14. There is a 3.3 dB increase in signal at the focal point compared to far-field scanning.

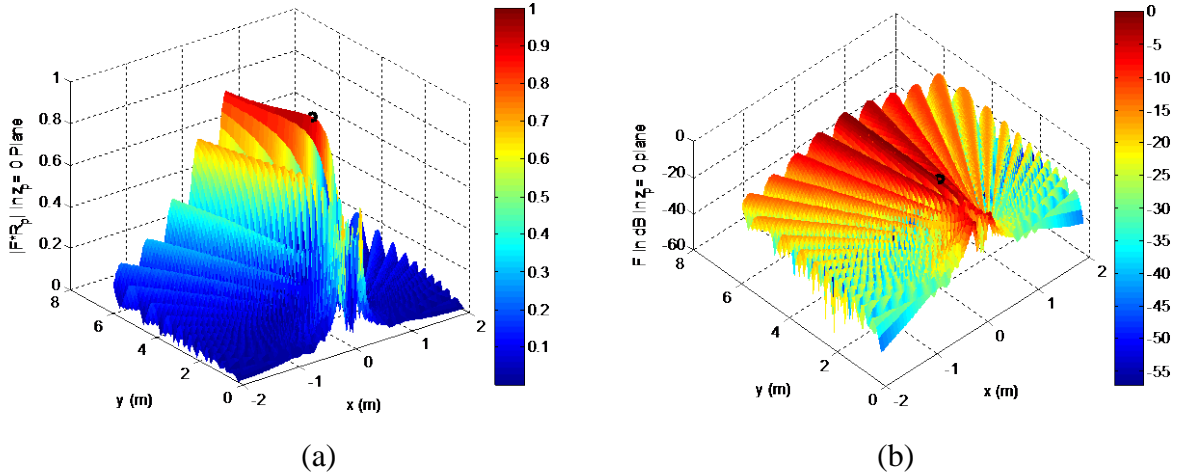


Figure 13. (a) Plots of normalized electric field in V/m and (b) in dBV/m when the array is focused at 2 m.

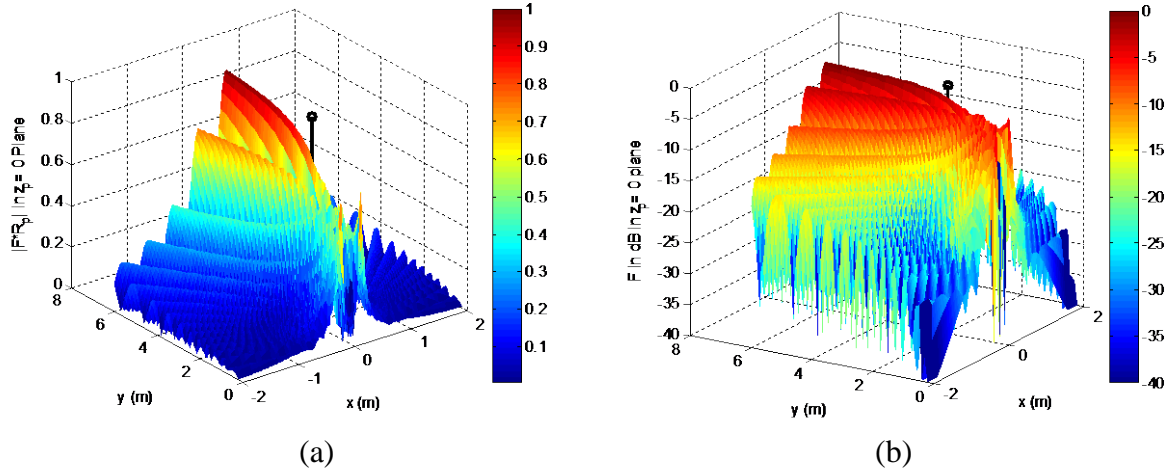


Figure 14. (a) Plot of normalized electric field in V/m and (b) in dBV/m when the array is focused at $z = 2000$ m (i.e., the far field). The $1/R$ factor has been removed.

2. Receiving Array

Let a receiving array be centered on the y axis at y_{p_0} with numbers of elements in the x and z directions of N'_x by N'_z and spacings d'_x and d'_z . Similar to the transmitting array the element locations are given by $x'_{pq} = \frac{2p - (N'_x + 1)}{2} d'_x$, $z'_{pq} = \frac{2q - (N'_z + 1)}{2} d'_z$ and $y'_{pq} = 0$ ($1 \leq p \leq N'_x$, $1 \leq q \leq N'_z$) as shown in Figure 15. The primed quantities and indices p and q are associated with the receive array.

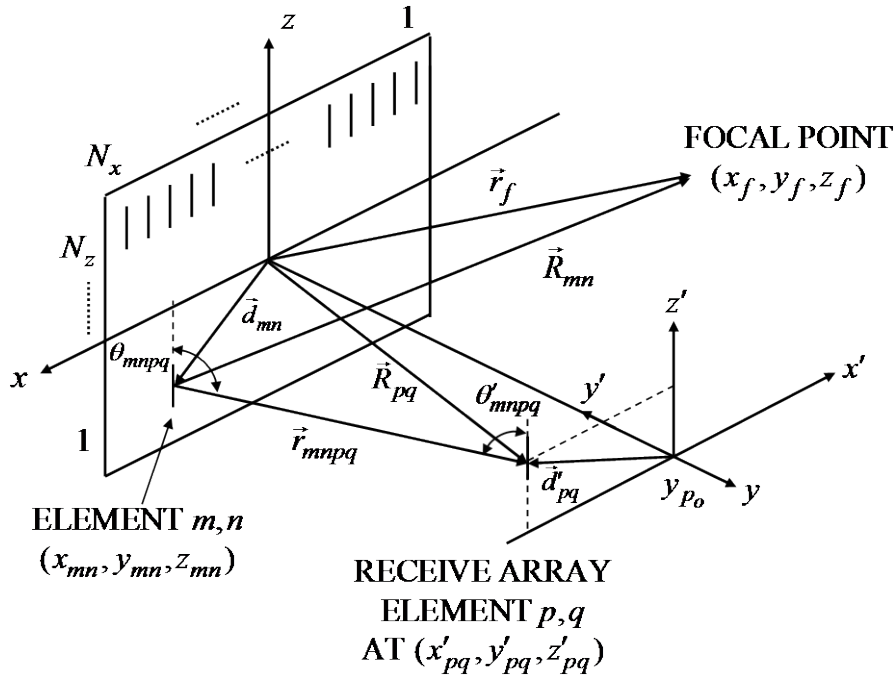


Figure 15. Total field at element p, q of a receiving array.

The incident field at element p,q is obtained by setting its location as the field point in Figure 12:

$$\vec{E}^i(R, \theta, \phi) \rightarrow \vec{E}^i(x'_{pq}, y'_{pq}, z'_{pq}) \equiv \vec{E}^i_{pq}.$$

The total field at element p,q due to all elements in the transmitting array is given by Eq. (14) with the appropriate angles and distances inserted

$$\vec{E}^i_{pq} = j120 \hat{z} \sum_{m=1}^{N_x} \sum_{n=1}^{N_y} \left\{ \frac{e^{-j\beta r_{mnpq}}}{r_{mnpq}} f(\theta_{mnpq}, \phi_{mnpq}) A_{mn} e^{j\Phi_{mn}} e^{j\psi_{mn}} \right\} \quad (17)$$

where

$$\vec{r}_{mnpq} = (x_{pq} - x_{mn})\hat{x} + (y_{pq} - y_{mn})\hat{y} + (z_{pq} - z_{mn})\hat{z}. \quad (18)$$

$r_{mnpq} = |\vec{r}_{mnpq}|$ and θ_{mnpq} is the angle of the axis of transmitting element m,n with the LOS vector to receive element p,q (an extension of Eq. (11))

$$\cos(\theta_{mnpq}) = \frac{\vec{r}_{mnpq} \cdot \hat{z}}{|\vec{r}_{mnpq}|}. \quad (19)$$

Similarly extending Eq. (12), the azimuth angle is

$$\tan(\phi_{mnpq}) = \frac{y_{pq} - y_{mn}}{x_{pq} - x_{mn}}. \quad (20)$$

The complex voltage out of receiving element p,q is given by

$$V_{pq} = \vec{E}^i_{pq} \cdot \vec{h}_{pq}(\theta'_{mnpq}, \phi'_{mnpq}) \quad (21)$$

where \vec{h}_{pq} is the vector effective height of receive element p,q and $(\theta'_{mnpq}, \phi'_{mnpq})$ the direction from the receive element axis with the LOS to transmit element m,n

$$\cos(\theta'_{mnpq}) = \frac{\vec{r}_{mnpq} \cdot \hat{z}'_{pq}}{|\vec{r}_{mnpq}|} \quad (22)$$

$$\tan(\phi'_{mnpq}) = \frac{y'_{mn} - y'_{pq}}{x'_{mn} - x'_{pq}}. \quad (23)$$

Note that the axes of the receiving array (primed) are related to those of the transmitting array by

$$\hat{z}' = \hat{z}, \hat{x}' = -\hat{x}, \hat{y}' = -\hat{y} \quad (24)$$

and for every point

$$z' = z, x' = -x, y' = -y. \quad (25)$$

For a half-wave dipole on the z' axis over a PEC ground, the effective height is derived in the Appendix:

$$\bar{h}_{pq} = -j \frac{4}{\beta} f(\theta'_{mnpq}, \phi'_{mnpq}) \hat{\theta}'. \quad (26)$$

This is an idealized result for an isolated element above an infinite ground plane. The effective height of a dipole over a finite ground plane or in an array environment will differ from this due to mutual coupling and diffraction.

The final step is to calculate the total complex voltage at the output of the receive array, which is the complex sum of all receiving dipole voltages

$$\begin{aligned} V_{\text{out}} &= \sum_{p=1}^{N'_x} \sum_{q=1}^{N'_z} V_{pq} A'_{pq} e^{j\psi'_{pq}} \\ &= j \frac{480}{\beta} \sum_{p=1}^{N'_x} \sum_{q=1}^{N'_z} \sum_{m=1}^{N_x} \sum_{n=1}^{N_z} \left\{ \hat{z} \square \hat{\theta}'_{pq} h_{pq}(\theta'_{mnpq}, \phi'_{mnpq}) A'_{pq} e^{j\psi'_{pq}} \right. \\ &\quad \left. \times \Psi(r_{mnpq}) f(\theta_{mnpq}, \phi_{mnpq}) A_{mn} e^{j\Phi_{mn}} e^{j\psi_{mn}} \right\} \end{aligned} \quad (27)$$

where A'_{pq} and ψ'_{pq} are miscellaneous calibration and correction amplitudes and phases applied on receive, if any. $\hat{\theta}'_{pq}$ is the unit vector in the spherical system centered at p, q . Given that Eqs. (23) hold

$$\hat{z} \square \hat{\theta}'_{pq} = -\sin \theta'_{mnpq}. \quad (28)$$

The final result for both arrays with half-wave dipoles above a PEC ground plane is

$$\begin{aligned} V_{\text{out}} &= j \frac{480}{\beta} \sum_{p=1}^{N'_x} \sum_{q=1}^{N'_z} A'_{pq} e^{j\psi'_{pq}} \left\{ \sum_{m=1}^{N_x} \sum_{n=1}^{N_z} \sin \theta'_{mnpq} \left(\frac{e^{-j\beta r_{mnpq}}}{r_{mnpq}} \right) \left[\frac{\cos\left(\frac{\pi}{2} w_{mnpq}\right)}{\sqrt{1-w_{mnpq}^2}} \sin(\beta h v_{mnpq}) \right] \right. \\ &\quad \left. \times A_{mn} e^{j\Phi_{mn}} e^{j\psi_{mn}} \left[\frac{\cos\left(\frac{\pi}{2} w'_{mnpq}\right)}{\sqrt{1-(w')_{mnpq}^2}} \sin(\beta h v'_{mnpq}) \right] \right\} \end{aligned} \quad (29)$$

where

$$\begin{aligned} v_{mnpq} &= \sin \theta_{mnpq} \sin \phi_{mnpq} \\ w_{mnpq} &= \cos \theta_{mnpq}, \quad \sin \theta_{mnpq} = \sqrt{1-w_{mnpq}^2} \\ v'_{mnpq} &= \sin \theta'_{mnpq} \sin \phi'_{mnpq} \\ w'_{mnpq} &= \cos \theta'_{mnpq}, \quad \sin \theta'_{mnpq} = \sqrt{1-(w')_{mnpq}^2}. \end{aligned} \quad (30)$$

Note that in Eq. (29) the voltages of the elements have been summed (i.e., series combination). For parallel combination the voltage is constant and we should use $V_{\text{out}} / (N'_x N'_z)$. The time-average power is

$$\begin{aligned} P_L &= \frac{1}{2} \text{Re} \{ V I^* \} \\ &= \frac{1}{2(N'_x N'_z)} \text{Re} \{ V_{\text{out}} I_{\text{out}}^* \}. \end{aligned} \quad (31)$$

The power delivered to a conjugate matched receiving load of resistance R_L is [6]

$$P_L = \frac{|V_{\text{out}}|^2}{(N'_x N'_z) 8 R_L}. \quad (32)$$

C. SIMULATION RESULTS

Several benchmark cases were run to validate the software written in Matlab. For the validation purposes only, a frequency of 300 MHz is used. The commercial software package Savant was used to compute the power transferred between a 10 by 10 transmitting array and the receiving antenna (see Figure 16).

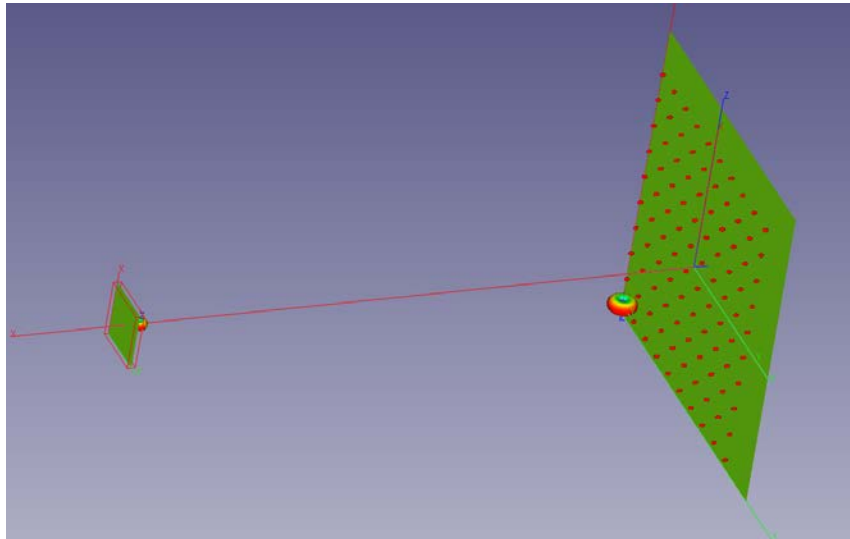
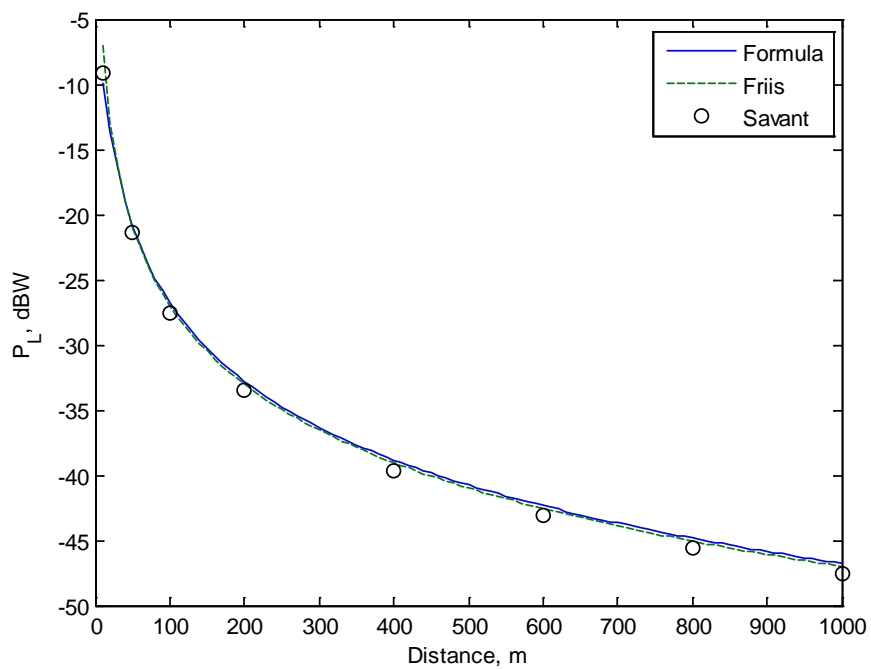
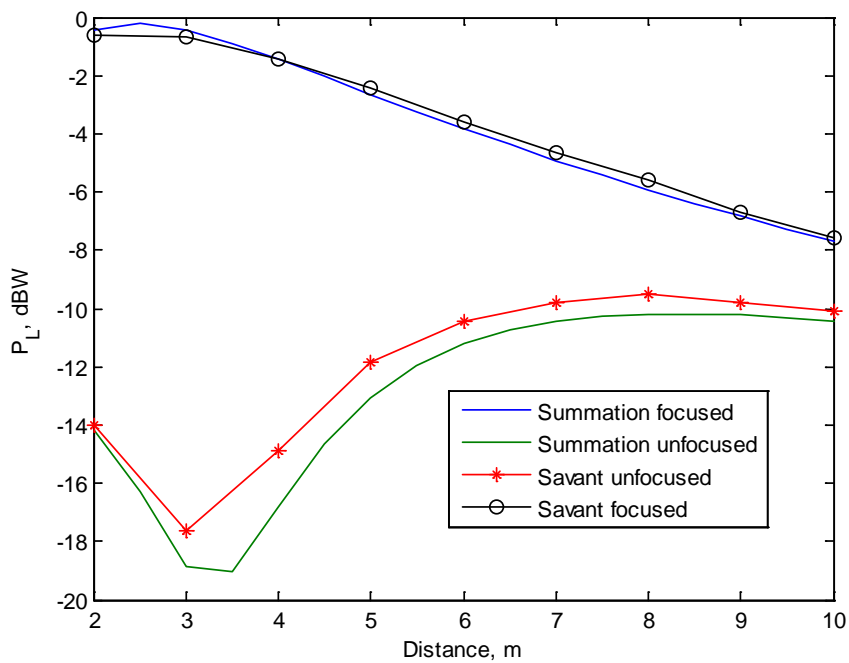


Figure 16. Savant model of the transmitting array and receiving antenna.

A comparison of the results is shown for ranges greater than 10 m in Figure 17(a). Equation (2), the Matlab results for Eqs. (29) – (32), and the Savant simulation are all in good agreement. The far field condition is assumed to hold – there are no phase corrections for focusing. A comparison of the focused and unfocused cases is shown in Figure 17(b). The focused case gives an improvement of 12 dB or more at ranges less than 3 m. This confirms the results presented previously in Figure 13.



(a)



(b)

Figure 17. Power received by a single dipole over a ground plane from a 10 by 10 array with ground plane transmitting 1 W. (a) Comparison of summation formula to Friis and Savant simulations (no focusing). (b) Comparison of summation formula to Savant simulations for near field ranges with and without focusing.

THIS PAGE INTENTIONALLY LEFT BLANK

IV. SUMMARY, CONCLUSIONS AND FUTURE WORK

The inductive and radiative approaches to WPT were simulated using commercial software. For the inductive approach, working at 100 kHz, efficiencies over 90% were achieved at short ranges (less than 30 mm) utilizing ferrite plates. For the radiative approach, the transmission loss between antennas was less than 1 dB at ranges less than 3 m when near field focusing was employed. The results for the two approaches are important because they demonstrate that efficient transmission of energy can take place between the WPT ground station and client.

The frequency used in the simulations was 300 MHz, however the efficiency conclusions apply to other frequencies when the antennas are scaled in wavelengths. For example, the 10 by 10 array with ground plane is approximately 5 m square at 300 MHz, but would reduce to 0.5 m square at 3 GHz, or 0.15 m square at 10 GHz.

The next step in the research (Phase II) is to design efficient rectifying and battery charging circuits. Candidate designs can be simulated using the commercial software package Advanced Design System (ADS) from Keysight (formerly Agilent). Rectifier efficiencies of 90% have been reported at low frequencies (< 10 MHz) because efficient diodes are available in this range. However, at higher frequencies, (e.g., 10 GHz), achieving this level of efficiency is more difficult [7, 8].

THIS PAGE INTENTIONALLY LEFT BLANK

APPENDIX A. EFFECTIVE HEIGHT OF A HALF-WAVE DIPOLE OVER A GROUND PLANE

Consider element m,n to be a z directed dipole at a height h above a ground plane that is located in the x - z plane. The ground plane factor is

$$GPF = e^{j\beta h \cos \alpha_{y_{mn}}} - e^{-j\beta h \cos \alpha_{y_{mn}}} = 2j \sin(\beta h \cos \alpha_{y_{mn}})$$

where $\cos \alpha_{y_{mn}} = v_{mn} = \sin \theta_{mn} \sin \phi_{mn}$ is the y direction cosine. The element factor for a z dipole over the ground plane is

$$\begin{aligned} EF_{mn} &= \hat{z} 2j \sin(\beta h \sin \theta_{mn} \sin \phi_{mn}) \left(j60 \frac{e^{-j\beta r_{mn}} \cos\left(\frac{\pi}{2} \cos \theta_{mn}\right)}{r_{mn} \sin \theta_{mn}} \right) \\ &= -120 \hat{z} \frac{e^{-j\beta r_{mn}}}{r_{mn}} \sin(\beta h v_{mn}) \frac{\cos\left(\frac{\pi}{2} w_{mn}\right)}{\sqrt{1-w_{mn}^2}}. \end{aligned}$$

The effective height is determined from

$$V_{mn} = \vec{E}_{mn} \square \vec{h}_{mn}$$

and

$$\vec{E}_{mn} = -j\eta \frac{I\beta}{4\pi r} e^{-j\beta r} \vec{h}_{mn}.$$

For a half wave dipole with a ground plane:

$$\vec{h}_{mn} = -j \frac{4}{\beta} \frac{\cos\left(\frac{\pi}{2} \cos \theta_{mn}\right)}{\sin \theta_{mn}} \sin(\beta h \sin \theta_{mn} \sin \phi_{mn}) \hat{\theta}_{mn}.$$

Typically we choose $h = \lambda/4$ so that $\beta h = \pi/2$. This is an idealized far field result for an isolated element above an infinite ground plane. The effective height of a dipole over a finite ground plane, in an array environment, or in the near field is different from $\sin(\beta h \sin \theta_{mn} \sin \phi_{mn})$ due to mutual coupling and diffraction. These effects can be accounted for by modifying the ground plane factor to include an efficiency factor (A) and taper exponent (B) to match the actual behavior:

$$A \sin^B(\beta h \sin \theta_{mn} \sin \phi_{mn}).$$

THIS PAGE INTENTIONALLY LEFT BLANK

LIST OF REFERENCES

- [1] W. C. Brown, "The history of power transmission by radio waves," *IEEE Trans. Microw. Theory Tech.*, vol. MTT-32, no. 9, pp. 1230–1242, Sept. 1984.
- [2] F. Ulaby, "Maxwell's equations for time-varying fields," in *Fundamentals of applied electromagnetics*, 5th ed. Upper Saddle River: Pearson Prentice Hall, ch. 6, pp. 255–270, 2007.
- [3] J. Cena, "Power Transfer Efficiency of Mutually Coupled Coils in an Aluminum AUV Hull," Masters Thesis, Naval Postgraduate School, December 2013.
- [4] V. Bana, G. Anderson, L. Xu, D. Rodriguez, A. Phipps and J. Rockway, "Characterization of coupled coils in seawater for wireless power transfer," SPAWAR, San Diego, CA, Tech. Rep. 2026, 2013.
- [5] Hiroshi Matsumoto, "Research on Solar Power Satellites and Microwave Power Transmission in Japan," *IEEE Microwave Magazine*, December 2002, pp. 36-45.
- [6] C. Balanis, *Antenna Theory, Analysis and Design*, 2nd edition, 1997, Wiley.
- [7] James O. McSpadden, Lu Fan and Kai Chang, "Design and Experiments of a High-Conversion-Efficiency 5.8-GHz Rectenna," *IEEE Transaction on Microwave Theory and Techniques*, Vol. 46, No. 12, Dec 1998.
- [8] Tae-Whan Yoo and Kai Chang, "Theoretical and Experimental Development of 10 and 35 GHz Rectennas," *IEEE Transactions on Microwave Theory and Techniques*, Vol. 40, No. 6, June 1992.

THIS PAGE INTENTIONALLY LEFT BLANK

INITIAL DISTRIBUTION LIST

1. Defense Technical Information Center
Ft. Belvoir, Virginia
2. Dudley Knox Library
Naval Postgraduate School
Monterey, California
3. Research Sponsored Programs Office, Code 41
Naval Postgraduate School
Monterey, CA 93943